Nuclear Engineering and Technology 53 (2021) 1304–1310

Contents lists available at ScienceDirect

Nuclear Engineering and Technology

journal homepage: www.elsevier.com/locate/net

Original Article

# Development of a novel reconstruction method for two-phase flow CT with improved simulated annealing algorithm

Mingfei Yan [a], Huasi Hu [a, *], Guang Hu [a], Bin Liu [b], Chao He [c], Qiang Yi [c]

[a] School of Energy and Power Engineering, Xi 'an Jiaotong University, Xi 'an, 710049, China
[b] Science and Technology on Reactor System Design Technology Laboratory, Nuclear Power Institute of China, Chengdu, 610213, China
[c] Institute of Nuclear Physics and Chemistry, China Academy of Engineering Physics, Mianyang, 621900, China

ARTICLE INFO

*Article history:*
Received 3 March 2020
Received in revised form
10 August 2020
Accepted 16 September 2020
Available online 21 September 2020

*Keywords:*
Two-phase flow
Neutron CT
Image reconstruction
Simulated annealing algorithm

ABSTRACT

Two-phase flow, especially gas-liquid two-phase flow, has a wide application in industrial field. The diagnosis of two-phase flow parameters, which directly determine the flow and heat transfer characteristics, plays an important role in providing the design reference and ensuring the security of online operation of two-phase flow system. Computer tomography (CT) is a good way to diagnose such parameters with imaging method. This paper has proposed a novel image reconstruction method for thermal neutron CT of two-phase flow with improved simulated annealing (ISA) algorithm, which makes full use of the prior information of two-phase flow and the advantage of stochastic searching algorithm. The reconstruction results demonstrate that its reconstruction accuracy is much higher than that of the reconstruction algorithm based on weighted total difference minimization with soft-threshold filtering (WTDM-STF). The proposed method can also be applied to other types of two-phase flow CT modalities (such as X(γ)-ray, capacitance, resistance and ultrasound).


## 1. Introduction

Gas-liquid two-phase flow widely exists in petrochemical engineering, nuclear power plant, thermal power generation and aerospace fields. The two-phase flow parameters, such as void fraction, density and flow flux, have significant influence on flow and heat transfer characteristics of two-phase flow. The accurate diagnosis of the two-phase flow parameters not only can provide an important design reference but also guarantee the security of online operation of the equipment, which keeps a hot and hard research issue.

In general, radiation (X(γ)-ray and neutron) class [1], optical class [2], electrical class [3], and ultrasonic class [4] methods can be applied to diagnose the two-phase flow parameters, among which radiation class method can achieve satisfactory results under reasonable cost due to the advantages of nonintrusive and hard field characteristics. Early in 1965, J. B. Romero et al. have utilized flash X-ray radiography to observe the void behavior in fluidized bed [5]. As the development of medical imaging technology, CT has successively applied in diagnosing two-phase flow parameters. For example, S. Morooka et al. used X-ray CT scanner to measure the void fraction in a simulated boiling water reactor (BWR) fuel assembly in 1989 [6]. However, such CT scanner is only suitable for steady state two-phase flow with X-ray tube and detector arrays rotating around void fraction measurement section. To improve the real-time performance of two-phase CT, G. A. Johansen et al. suggested a typical imaging configuration in 1996 [7], which mainly consists of five $^{241}$Am isotope radioactive sources and five CdZnTe semiconductor detector arrays, realizing collecting the projection data in every directions at the same time. From then on, X-ray CT applied in two-phase flow visualization has already made great strides [8,9]. Compared with X(γ)-rays, neutron has larger macroscopic cross section difference between water and air, and further provides a larger contrast to noise ratio (CNR) on the image [10]. Therefore, it shows potential advantages in visualizing two-phase flow. R. Zbory et al. in Paul Scherrer Institute (PSI) initially visualized the two-phase flow in a model of boiling BWR fuel rod bundle via neutron CT in 2011 [10], and their research scope ranged from cold neutron CT to fast neutron CT in successive work [11,12].

This paper employs the similar imaging configuration proposed by G. A. Johansen for real time imaging with thermal neutrons. The developed reconstruction algorithm based on it can be directly extended to other two-phase CT modalities (such as X(γ)-ray,

* Corresponding author.
*E-mail address:* huasi_hu@mail.xjtu.edu.cn (H. Hu).

https://doi.org/10.1016/j.net.2020.09.021

capacitance, resistance and ultrasound). In the configuration of thermal neutron CT of two-phase flow, the number of projection data is extremely limited, which especially requires the high performance image reconstruction algorithms. Theoretically, any of the CT image reconstruction algorithms suitable for sparse sampling problem can be directly applied to two-phase flow CT reconstruction, such as typical simultaneous algebraic reconstruction technique (SART) [13], maximum likelihood expectation maximization (MLEM) [14], the sparse algorithm based on total variation minimization (TVM) [15] and the sparse algorithm based on weighted total difference minimization (WTDM) [16,17]. However, the algorithms can show better performance if the prior information of reconstructed object can be integrated into the reconstruction process. Heuristic algorithms, mainly include genetic algorithm [18], ant colony optimization (ACO) [19], simulated anneal (SA) [20] and artificial neural network (ANN) [21], are widely used in optimization design field, which show evident advantages in solving large and complex space problem, especially for non-deterministic polynomial (NP) hard problem. Moreover, the prior information of reconstructed image can be integrated into it conveniently when they are applied to image reconstruction. Therefore, such kind of algorithms have potential advantages for CT image reconstruction under sparse sampling. X. G. Yang et al. have successfully applied GA to two-phase CT reconstruction [22]. Its reconstruction accuracy has exceeded that of filter back projection (FBP) and SART algorithms. Inspired by their work, we have developed a novel reconstruction method for thermal neutron CT of two-phase flow with SA algorithm.

## 2. Mathematic principle of neutron CT

The configuration of thermal neutron CT of two-phase flow is shown in Fig. 1, which mainly consists of five neutron sources, five groups of front and back collimators, five groups of detector arrays and a two-phase flow pipeline. The neutron source energy is 25.3 meV. The material of collimators is $B_4C$, which has high efficiency to absorb the scattered thermal neutrons with small size. In order to decrease the integration time for a tomography image, larger pixel size on the detector array is expected. The pixel size is 4 mm × 4 mm × 0.05 mm (thickness), and the material of the pixel is $^6$LiF (ZnS: Ag). Each groups of detector array contains 37 such pixels. Because the number of total pixels in this configuration is only 185 (5 × 37), it is a typical sparse sampling problem, and high reconstruction accuracy is hard to be achieved. However, the interpolation method can be used to increase the number of projection data, and further improve the reconstruction accuracy. In this paper, we set virtual pixels to extend the number of pixels from 37 to 451, and the projection data acquired by each virtual pixel is determined by cubic interpolation.

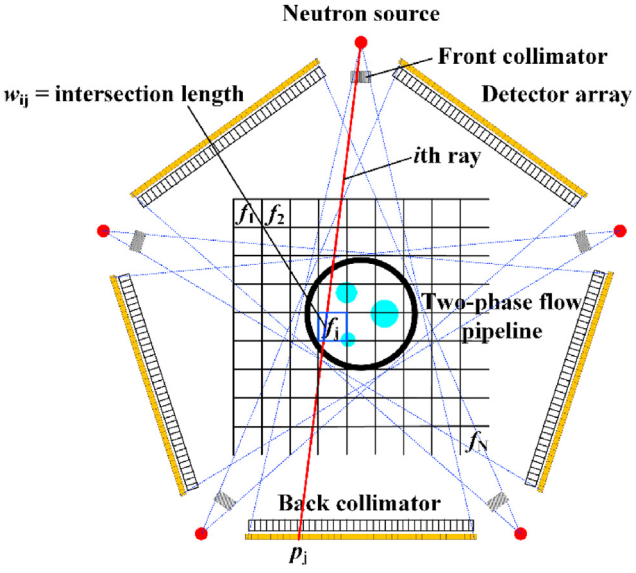


**Fig. 1.** Configuration of thermal neutron CT of two-phase flow.

Similar as X(γ)-ray, narrow neutron beam interaction with the matter follows Lambert-Beer law:

$$I(x,y) = I_0(x,y)e^{-\int_L f(x,y)dl} \tag{1}$$

Where $I_0(x,y)$ and $I(x,y)$ denote the incident and transmitted neutron intensities in the location $(x,y)$ respectively; $f(x,y)$ denotes the linear attenuation coefficient of neutron in the matter. From equation (1), it can be deduced out:

$$P(x,y) = \ln\left(\frac{I_0(x,y)}{I(x,y)}\right) = \int_L f(x,y)dl \tag{2}$$

Where $P(x,y)$ is termed as projection data in CT field. If we collect much projection data in different projection directions, the distribution of linear attenuation coefficient $f(x,y)$ can be restored (or reconstructed) by solving the equations constructed with equation (2) in different projection directions. If we utilize iteration class algorithms to implement the reconstruction, such equations can be regarded as a linear one:

$$\begin{bmatrix} p_1 \\ p_2 \\ \vdots \\ p_j \\ \vdots \\ p_M \end{bmatrix} = \begin{bmatrix} w_{11} & w_{12} & \cdots & w_{1j} & \cdots & w_{1\,N} \\ w_{21} & w_{22} & \cdots & w_{2j} & \cdots & w_{2\,N} \\ \vdots & \vdots & & \vdots & & \vdots \\ w_{i1} & w_{i2} & \cdots & w_{ij} & \cdots & w_{iN} \\ \vdots & \vdots & & \vdots & & \vdots \\ w_{M1} & w_{M2} & \cdots & w_{Mj} & \cdots & w_{MN} \end{bmatrix} \begin{bmatrix} f_1 \\ f_2 \\ \vdots \\ f_j \\ \vdots \\ f_N \end{bmatrix} \tag{3}$$

Where $[p_1, p_2, \ldots, p_j, \ldots, p_M] \in R^M$ is the projection vector (abbreviation $\boldsymbol{P}$) (M is the number of rays or detector pixels), which is simulated by MCNPX, and ENDF/B-Ⅶ is used as the database; $(w_{ij}) \in R^M \times R^N$ is termed as system matrix ($\boldsymbol{W}$) (N is the number of pixels on the reconstructed image), in which $w_{ij}$ refers to the contribution of the $j$th pixel to the line integration of the $i$th ray along its through path, and we assume the intersection length shown in Fig. 1 as the contribution; $[f_1, f_2, \ldots, f_j, \ldots, f_N] \in R^N$ is the image vector ($\boldsymbol{F}$) to be reconstructed. Therefore, CT image reconstruction is to seek the image vector from the projection vector and the system matrix, which can also be termed as solving the inverse problem. Different from well-posed equations, rank($\boldsymbol{W}$) = rank($\boldsymbol{W}|\boldsymbol{P}$)<N ($\boldsymbol{W}$ and $\boldsymbol{W}|\boldsymbol{P}$ are termed as the coefficient matrix and augmented matrix in linear equations respectively) is the usual case in CT image reconstruction, especially in sparse sampling case, and the equations is undetermined. The key issue in developing CT image reconstruction algorithm is to construct the method to solve the undetermined equations.

## 3. Improved simulated annealing algorithm

SA algorithm is a kind of stochastic searching algorithm based on Monte Carlo iterative solution strategy, and its start point is based on the similarity between the annealing process of solid material in physics and the generally combinatorial optimization problem. The principle of solid annealing is: firstly, the solid is heated to be high temperature state, particles in the solid become

disordered as the temperature rising, and the internal energy of the solid increases; secondly, particles incline to become ordered as cooling, and the internal energy of the solid decreases, then it can reach to the equilibrium state at each temperature; finally, it reaches to the ground state at room temperature, and the internal energy of the solid decrease to be minimum. In general, SA algorithm initiates from a relatively high temperature, and randomly searches globally optimal solution with the probabilistic jump characteristic in the solution domain as the temperature decreases.

The key points of constructing CT image reconstruction algorithms based on SA algorithm lie to constructing: the objective function, the new solution generation strategy, the probabilistic acceptance function and the initial temperature.

The objective function in this paper is:

$$\min\left(\|P-\mathrm{WF}\|_2^2+\omega\cdot\mathrm{WTD}(F)\right) \tag{4}$$

Where $\|P-\mathrm{WF}\|_2$ is the $l2$-normal of vector $P-\mathrm{WF}$; $\omega$ is a positive weight coefficient. $\mathrm{WTD}(F)$ is the weighted total difference of matrix $\boldsymbol{F}$; $\boldsymbol{P}$, $\boldsymbol{W}$ and $\boldsymbol{F}$ are the projection vector, system matrix and image vector described in section 2. The above objective function not only considers the accordance of reconstructed image with projection data, but also considers the sparse feature of the image, which has been proved to be an effective away to increase the reconstruction accuracy under the same number of projection data.

The idea of WTD comes from total difference (TD) of the image [17]. WTD describes the sparsity of the image in horizontal and vertical directions as well as diagonal ones (Fig. 2), which is expressed as:

$$\mathrm{WTD}(F)=\sum_{\mathrm{i}}\sum_{\mathrm{j}}\left(\left|f_{\mathrm{i+1,\,j}}-f_{\mathrm{i,\,j}}\right|+\left|f_{\mathrm{i,\,j+1}}-f_{\mathrm{i,\,j}}\right|+\alpha\left(\times\left|f_{\mathrm{i+1,\,j+1}}-f_{\mathrm{i,\,j}}\right|+\left|f_{\mathrm{i,\,j+1}}-f_{\mathrm{i+1,\,j}}\right|\right)\right) \tag{5}$$

The new solution generation strategy is extremely important in ISA algorithm, which directly determines the reconstruction efficiency and accuracy. Gas liquid two-phase flow is constituted of gas and liquid (gas is air and liquid is water in most cases), and the pixel value on the reconstructed image refers to the linear attenuation coefficient of neutron in the matter, so it can be thought to be 0 for air part and 1 for water part. The pixel value only can change from 0 to 1 or 1 to 0, which is termed as two-phase flow has binary characteristic. ISA with utilization of such feature can provide a higher probability for obtaining relatively high reconstruction accuracy under extremely limited number of projection data. The new solution in ISA algorithm is basically produced by inversing the pixel value (from 0 to 1, or 1 to 0) at the random location on the reconstructed image. Two-phase flow also has continuous characteristic, namely, air and water parts in two-phase flow usually contain at least two pixels. By means of its continuous characteristic, we regard the unknown pixel value is determined by its neighborhood pixels with a certain probability. Fig. 3 shows the neighborhood situation of each pixel on the reconstructed image. Here we take pixel $f_{\mathrm{i,\,j}}$ as an example to describe how to include the continuous characteristic of reconstruction object into the image reconstruction process, in which we regard the pixel value of $f_{\mathrm{i,\,j}}$ is unknown, and the pixel value of its 8 neighborhood pixels is known. If rand01() < $p_c$, the pixel vale of $f_{\mathrm{i,\,j}}$ is:

$$f_{\mathrm{i,\,j}}=\begin{cases}1, & \text{if rand01}()\ \le\ \mathrm{avg}\left(f_{\mathrm{i-1,\,j-1}},\ f_{\mathrm{i-1,\,j}},\ f_{\mathrm{i-1,\,j+1}},\ f_{\mathrm{i,\,j-1}},\ f_{\mathrm{i,\,j+1}},\ f_{\mathrm{i+1,\,j-1}},\ f_{\mathrm{i+1,\,j}},\ f_{\mathrm{i+1,\,j+1}}\right)\\ 0, & \text{else}\end{cases} \tag{6}$$

Where the function random01() produces a random number between 0 and 1; $p_c$ is a number between 0 and 1, which is one of the parameter in our proposed ISA algorithm; the function avg() calculates the average value of the pixels. The value of the pixel on the other positions, such as the corner pixel $f_{\mathrm{i\text{-}1,\,j\text{-}1}}$, the border pixel $f_{\mathrm{i,\,j\text{-}1}}$, and so on, can be determined by the similar method. The only different place is the number of their neighborhood pixels, which is 3 for pixel $f_{\mathrm{i\text{-}1,\,j\text{-}1}}$ and 5 for pixel $f_{\mathrm{i,\,j\text{-}1}}$.

The probabilistic acceptance for the new solution is the essence and significant feature of ISA algorithm, which is the outstanding advantage over deterministic algorithms, such as least square method and gradient descent method. By means of high performance probabilistic acceptance function, the algorithm has remarkable ability to escape from local optimum to global optimum:

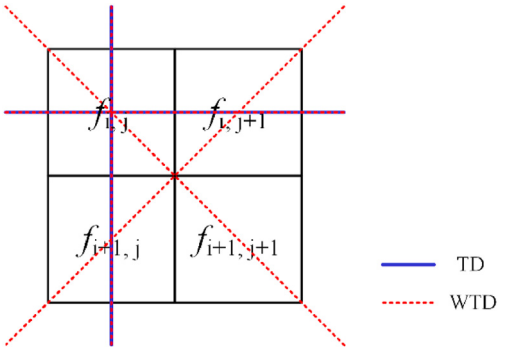


**Fig. 2.** Weighted total difference of the image.

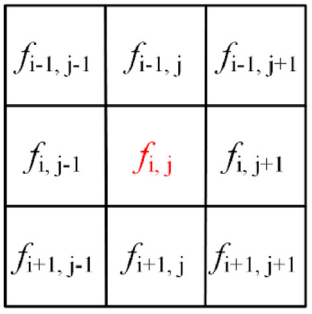


**Fig. 3.** Neighborhood situation of the pixel on the image.

$$p=\begin{cases}1, & \text{if } E(F')-E(F)\le 0\\ \exp\left(-\dfrac{E(F')-E(F)}{T(k)}\right), & \text{else}\end{cases} \tag{7}$$

Where $E(\Delta)$ denotes the objective function described in equation (4) regarding to the image vector $\Delta$; $F$ and $F'$ denote the old and new solution respectively; $T(k)$ is the cooling function, which is described as:

$$T(k)=\begin{cases}\dfrac{T_s}{\ln(k)}, & \text{if } k\le m\\ T_s{*}0.99^{k}, & \text{else}\end{cases} \tag{8}$$

Where $T_s$ is the initial temperature; $k$ is the number of annealing times; $m$ is a parameter in our developed ISA algorithm. Such cooling function is helpful for searching out the optimal solution with high efficiency.

The initial temperature $T_s$ has a great impact on the accuracy and efficiency in ISA algorithm. If it is too big, almost all the new solutions $F'$ making $E(F')-E(F)>0$ are accepted, thus the algorithm remains stagnant; if it is too small, almost all the new solutions $F'$ making $E(F')-E(F)>0$ are rejected, thus the algorithm becomes deterministic algorithm, which can't show the advantage of heuristic algorithm.

Based on the main parts of ISA algorithm described above, the flow chart of it is shown in Fig. 4: the image to be reconstructed and parameters in ISA algorithm are initialized; the new solution $F'$ is produced by randomly inversing the pixel value and changed with the continuous feature of two-phase flow; the probabilistic acceptance function is calculated and acceptance or rejection of the new solution $F'$ is judged, and the process is repeated until meeting the temporary equilibrium condition: the maximum number of iterations $N_i$; the temperature $T(k)$ decreases and the above processes are repeated until meeting the convergence condition: $T(k)<T_{stop}$.

The selection of parameters in CT image reconstruction algorithms is very important. After many attempts, a set of parameters are selected for ISA algorithm, which are suitable for all the phantoms in this paper: $\omega=5\times10^{-9}$, $\alpha=1$, $p_c=0.05$, $T_s=5$, $N_i=118803$, $m=15$, $T_{stop}=10^{-6}$.

## 4. Brief introduction to WTDM-STF algorithm

WTD is used as the sparsity term in our developed ISA algorithm, to make the comparison of the performance of ISA algorithm

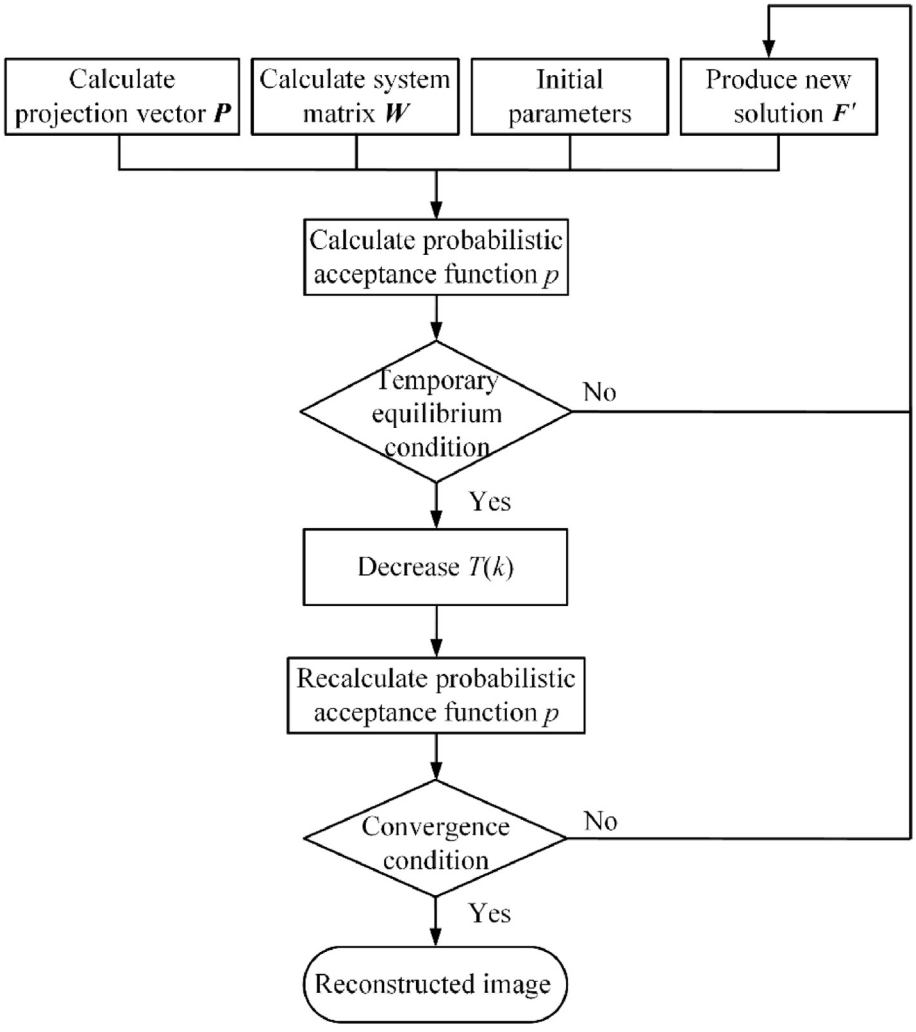


**Fig. 4.** Flow chart of ISA algorithm.

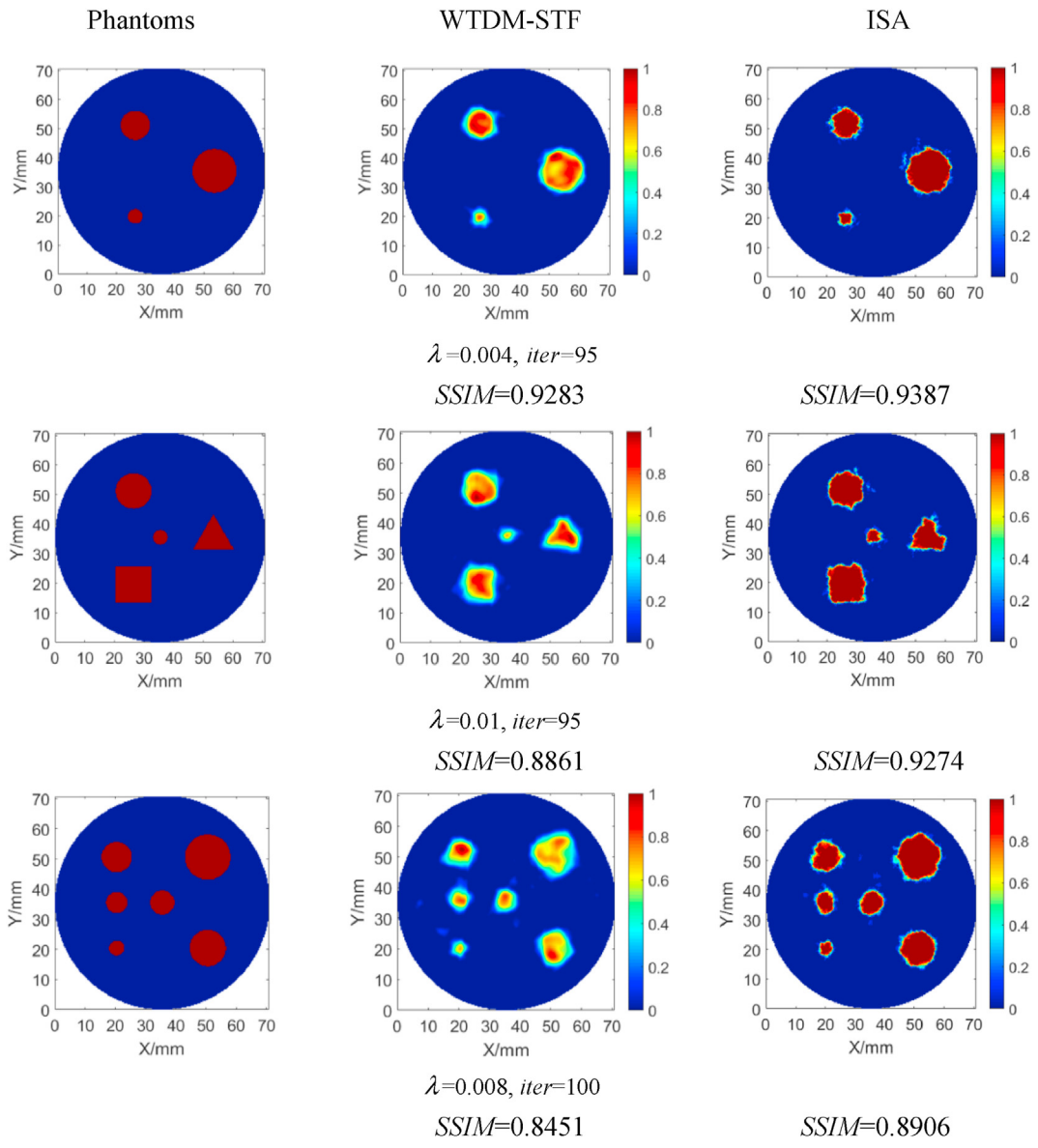


**Fig. 5.** Reconstructed results of phantoms with different complexity.

with other algorithm under a fair environment, the selection of algorithm participating in the comparison is extremely important. It is better to select the algorithm which employs the same sparsity term. Based on this principle, the newly developed WTDM-STF algorithm [17] is selected, which utilizes the same objective function as ISA algorithm. The different places are it uses SART algorithm to enforce the data consistency, and applies the soft-threshold filtering (STF) method to reduce the WTD of image, and adopts the fast iterative shrinkage thresholding algorithm (FISTA) to accelerate its convergence.

## 5. Reconstruction accuracy evaluation

To quantitatively evaluate the reconstruction accuracy of the image, the structural similarity (*SSIM*) [23] is used to measure the similarity between the reference and reconstructed images, which incorporates the luminance, contrast and structure information of the image:

$$SSIM(X,Y)=\frac{(2\mu_X\mu_Y+C_1)(2\sigma_{XY}+C_2)}{(\mu_X^2+\mu_Y^2+C_1)(\sigma_X^2+\sigma_Y^2+C_2)} \tag{9}$$

where $\mu_X$ and $\mu_Y$ denote the average of pixel value of image X and Y respectively; $\sigma_X$ and $\sigma_Y$ denote the standard deviation of them respectively; $\sigma_{XY}$ denotes the covariance of them; $C_1$ and $C_2$ are constants, which ensure the denominator is not zero, and they are zero in this paper. The bigger *SSIM* value is, the higher the reconstruction accuracy of the image is.

## 6. Reconstructed results

Apart from the type of selected algorithm participating in the comparison is important, the selection of parameters of it is also important. The best way to ensure the comparison under a fair environment is to make the algorithms work at best state with their optimal parameters, which can be obtained from sweeping out the whole parameter space. However, most of the algorithms have

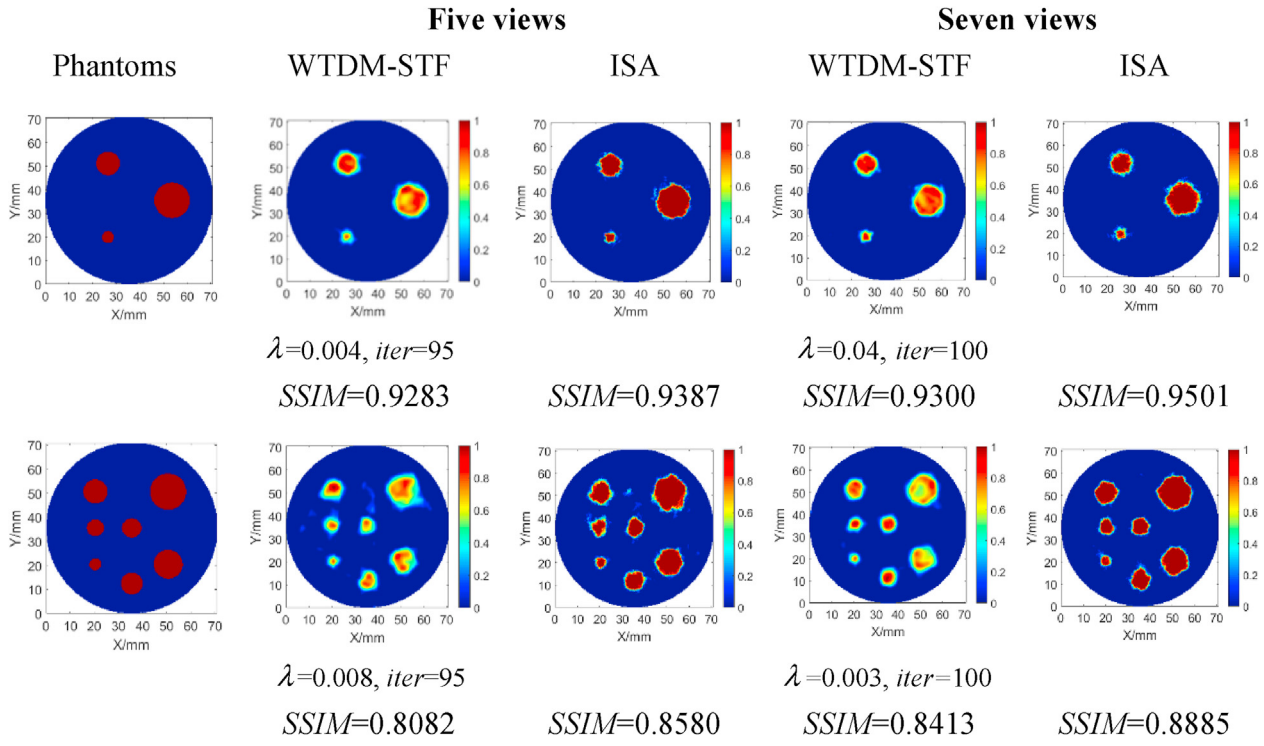


**Fig. 6.** Reconstructed results of phantoms under different number of views.

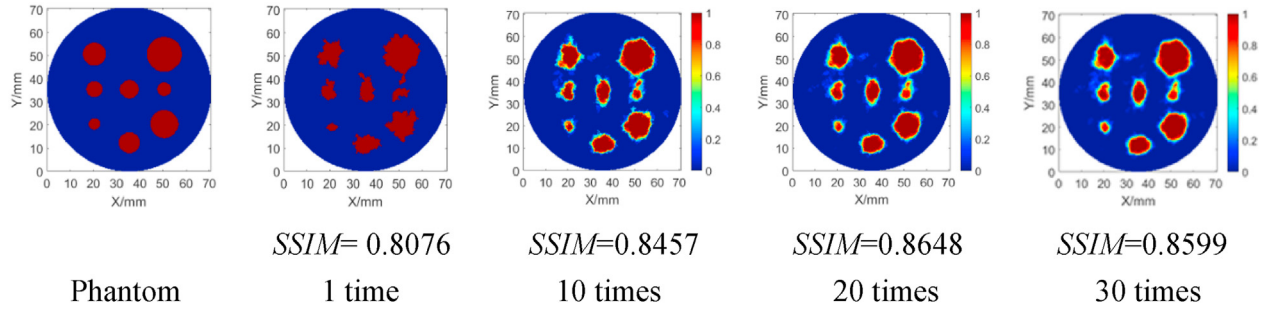


**Fig. 7.** Average image with different number of reconstructions.

more than one parameter, and the optimal parameters is different for different reconstructed objects, so sweeping out the whole parameter space is not realistic. In this paper, we select the optimal parameters for WTDM-STF algorithm one by one: when sweeping out the space of the relax factor $\lambda$, the iteration times *iter* keeps unchanged; after optimal $\lambda$ is determined, the optimal *iter* can be selected with the same method. The optimal parameters are determined by achieving the maximum *SSIM*. For ISA algorithm, as the description in section 3, we use the same set of parameters for all the phantoms. If the reconstruction accuracy of ISA algorithm can surpass WTDM-STF algorithm for different kinds of phantoms in this case, we can conclude that our developed ISA algorithm has better performance.

To better show the performance of ISA algorithm, we use two-phase flow phantoms with different "bubble" size, shape, location and quantity as the reconstructed objects, in which the smallest size of "bubble" is 5 mm. Fig. 5 shows the results reconstructed by ISA and WTDM-STF algorithms. For ISA algorithm results, we regard the average image of 10 reconstructions as the eventually reconstructed results. Generally speaking, the reconstruction accuracy of ISA algorithm is much higher than that of WTDM-STF algorithm for different phantoms. Specifically speaking, on one hand, compared with WTDM-STF algorithm, the central part of "bubbles" can be reconstructed more accurately by ISA algorithm. The main reasons are ISA algorithm just permits the pixel value changing from 0 to 1 or 1 to 0, and the continuous characteristic of two-phase flow has been utilized. On the other hand, for ISA algorithm results, the non-zero parts on the reconstructed "bubbles" almost only appear on the edge of "bubbles", which is caused by the average of 10 reconstructions. Such average is helpful for restoring the shape of "bubbles", and further significantly increases the reconstruction accuracy of the whole image. In addition, compared with WTDM-STF algorithm, the results provides a hint that the advantage of ISA algorithm tends to be more obvious as the complexity of the reconstructed objects increases.

We compare the reconstructed results of phantoms under different number of views, which is shown in Fig. 6. In two phase flow CT configuration (shown in Fig. 1), five views is utilized, however, it is possible to decrease or increase the number of views, such as three views, seven views and nine views. Basically,

decreasing the number of views results in the reconstruction accuracy decreasing, and vice versa. Here we compare five and seven views cases, and two phantoms (termed as three "bubbles" phantom and seven "bubbles" phantom) with different complexity are as the reconstructed objects. From the results, it can be observed that no matter for WTD-STF algorithm or ISA algorithm, increasing the number of views can significantly improve the reconstruction accuracy for both phantoms, especially for more complex seven "bubbles" phantom, the main reason is that more number of views is helpful for reconstructing the "bubble" shape; no matter for five views or seven views, the reconstruction accuracy of ISA algorithm is much higher than that of WTDM-STF algorithm, which further proves the performance of ISA algorithm is much better than that of WTD-STF algorithm.

As our mention in the contents above, ISA algorithm results are the average images of multiple reconstructions. Here we further discuss the influence of the number of reconstructions on the eventual reconstruction accuracy. Fig. 7 shows the reconstructed results of eight "bubbles" phantom with average of 1, 10, 20 and 30 reconstructions. It can be seen that the reconstruction accuracy of eventual images increases as the number increases from 1 to 20. The reason is that more number of images participating in the average can better suppress the artifacts on the eventual image. However, the reconstruction accuracy decreases as the number increases to 30. The reason is that the error generated in the average process has exceed the benefit it brings in. It is worth to mention that the optimal number of reconstructions participating in the average is related to the reconstructed object, which requires to be selected carefully.

## 7. Discussion and conclusion

We have proposed an ISA algorithm for two-phase flow CT reconstruction based on basic SA algorithm. In developing the algorithm, the mathematic model corresponding to the prior information of two-phase flow is constructed. Then we make the comparison of its reconstruction accuracy with WTDM-STF algorithm which has the same sparsity term WTD. The reconstruction results demonstrate that the reconstruction accuracy of ISA algorithm is much higher than that of WTDM-STF algorithm, which has great advantage in applying in two-phase flow CT reconstruction. The disadvantage of ISA is its higher time consumption than WTDM-STF algorithm. It is worth to mention that the proposed method can also be applied to other types of two-phase flow CT modalities (such as X($\gamma$)-ray, capacitance, resistance and ultrasound). In addition, the performance of ISA algorithm still have some space to be enhanced, for example, the new solution generation strategy and the cooling function can be further improved to get higher reconstruction accuracy and efficiency.

## Declaration of competing interest

The authors declare that they have no known competing financial interests or personal relationships that could have appeared to influence the work reported in this paper.

## Acknowledgments

The research is supported by the NSAF Joint Fund of China (Grant No. U1830128) and the National Natural Science Foundation of China (Grant No. 11975182 and 11875214).

## Appendix A. Supplementary data

Supplementary data to this article can be found online at https://doi.org/10.1016/j.net.2020.09.021.

## References

[1] C. Boyer, A.-M. Duquenne, G. Wild, Measuring techniques in gas-liquid and gas-liquid-solid reactors, Chem. Eng. Sci. 57 (2002) 3185–3215.
[2] E. Schleicher, M.J. Silva, S. Thiele, A. Li, E. Wollrab, U. Hampel, Design of an optical tomograph for the investigation of single- and two-phase pipe flows, Meas. Sci. Technol. 19 (2008), 094006.
[3] T. Wondrak, M. Soleimani, A novel metal flow imaging using electrical capacitance tomography, Meas. Sci. Technol. 28 (2017), 064001.
[4] L.C. Xing, Y.F. Geng, C.Q. Hua, H. Zhu, A. Rieder, W. Drahm, M. Bezdek, A combination method for metering gas-liquid two-phase flows of low liquid loading applying ultrasonic and Coriolis flowmeters, Flow Meas. Instrum. 37 (2014) 135–143.
[5] J.B. Romero, D.W. Smith, Flash x-ray analysis of fluidized beds, AIChE J. 11 (1965) 595–600.
[6] S. Morooka, T. Ishizuka, M. Iizuka, K. Yoshimura, Experimental study on void fraction in a simulated BWR fuel assembly (Evaluation of cross-sectional averaged void fraction), Nucl. Eng. Des. 114 (1989) 91–98.
[7] G.A. Johansen, T. Frøystein, B.T. Hjertaker, Ø. Olsen, A dual sensor flow imaging tomographic system, Meas. Sci. Technol. 7 (1996) 297–307.
[8] Q. Wang, H.X. Wang, Y. Yan, Fast reconstruction of computerized tomography images based on the cross-entropy method, Flow Meas. Instrum. 22 (2011) 295–302.
[9] S. Xin, H.X. Wang, Gamma-ray CT from incomplete projections for two-phase pipe flow, Rev. Sci. Instrum. 88 (2017), 025106.
[10] R. Zboray, J. Kickhofel, M. Damsohn, H.-M. Prasser, Cold-neutron tomography of annular flow and functional spacer performance in a model of a boiling water reactor fuel rod bundle, Nucl. Eng. Des. 241 (2011) 3201–3215.
[11] R. Zboray, H.-M. Prasser, Measuring liquid film thickness in annular two-phase flows by cold neutron imaging, Exp. Fluid 54 (2013) 1596.
[12] R. Zboray, R. Adams, M. Cortesi, H.-M. Prasser, Development of a fast neutron imaging system for investigating two-phase flows in nuclear thermal-hydraulic phenomena: a status report, Nucl. Eng. Des. 273 (2014) 10–23.
[13] A.H. Andersen, A.C. Kak, Simultaneous algebraic reconstruction technique (SART): a superior implementation of the ART algorithm, Ultrason. Imag. 6 (1984) 81–94.
[14] L.A. Shepp, Y. Vardi, Maximum likelihood reconstruction for emission tomography, IEEE Trans. Med. Imag. 1 (1982) 113–122.
[15] E.Y. Sidky, X.C. Pan, Image reconstruction in circular cone-beam computed tomography by constrained, total-variation minimization, Phys. Med. Biol. 53 (2008) 4777–4807.
[16] H.Y. Yu, G. Wang, A soft-threshold filtering approach for reconstruction from a limited number of projections, Phys. Med. Biol. 55 (2010) 3905–3916.
[17] W. Yu, L. Zeng, A novel weighted total difference based image reconstruction algorithm for few-view computed tomography, PLoS One 9 (2014), e109345.
[18] D. Whitley, A genetic algorithm tutorial, Stat. Comput. 4 (1994) 65–85.
[19] M. Dorigo, C. Blum, Ant colony optimization theory: a survey, Theor. Comput. Sci. 344 (2005) 243–278.
[20] S. Kirkpatrick, C.D. Gelatt Jr., M.P. Vecchi, Optimization by simulated annealing, Science 220 (1983) 4598.
[21] C.E. Floyd Jr., An artificial neural network for SPECT image reconstruction, IEEE Trans. Med. Imag. 10 (1991) 485–487.
[22] X.G. Yang, J. Ruud van Ommen, R.F. Mudde, Comparison of genetic algorithm and algebraic reconstruction for X-ray tomography in bubbling fluidized beds, Powder Technol. 253 (2014) 626–637.
[23] A. Horé, D. Ziou, Image quality metrics: PSNR vs. SSIM, Int. Conf. Pattern Recogn. 1 (2010) 2366–2369.